Polarization-Diversity Optical Coherence Tomography Assessment of Choroidal Nevi

Yusi Miao,[1] Hoyoung Jung,[2] Destiny Hsu,[3] Jun Song,[4] Shuibin Ni,[5] Da Ma,[6] Yifan Jian,[5] Shuichi Makita,[7] Yoshiaki Yasuno,[7] Marinko V. Sarunic,[3,8,9] Kirk A. J. Stephenson,[1] Katherine Paton,[1] Zaid Mammo,[1] and Myeong Jin Ju[1,4]

[1]Department of Ophthalmology and Visual Sciences, University of British Columbia, Vancouver, British Columbia, Canada
[2]Faculty of Medicine, University of British Columbia, Vancouver, British Columbia, Canada
[3]School of Engineering Science, Simon Fraser University, Burnaby, British Columbia, Canada
[4]School of Biomedical Engineering, University of British Columbia, Vancouver, British Columbia, Canada
[5]Case Eye Institute, Oregon Health & Science University, Portland, Oregon, United States
[6]Gerontology and Geriatric Medicine, Wake Forest University School of Medicine, Winston-Salem, North Carolina, United States
[7]Faculty of Medicine, University of Tsukuba, Tsukuba, Ibaraki, Japan
[8]Department of Medical Physics and Biomedical Engineering, University College London, London, England, United Kingdom
[9]Institute of Ophthalmology, University College London, London, England, United Kingdom

Correspondence: Myeong Jin Ju and Zaid Mammo, 2550 Willow Street, Vancouver, BC V5Z 3N9, Canada; myeongjin.ju@ubc.ca, zaid.mammo@ubc.ca.

YM and HJ contributed equally to this work.

Received: March 30, 2023
Accepted: October 9, 2023
Published: November 6, 2023

Citation: Miao Y, Jung H, Hsu D, et al. Polarization-diversity optical coherence tomography assessment of choroidal nevi. *Invest Ophthalmol Vis Sci.* 2023;64(14):6. https://doi.org/10.1167/iovs.64.14.6

Purpose. The purpose of this study was to demonstrate the utility of polarization-diversity optical coherence tomography (PD-OCT), a noninvasive imaging technique with melanin-specific contrast, in the quantitative and qualitative assessment of choroidal nevi.

Methods. Nevi were imaged with a custom-built 55-degree field-of-view (FOV) 400 kHz PD-OCT system. Imaging features on PD-OCT were compared to those on fundus photography, auto-fluorescence, ultrasound, and non-PD-OCT images. Lesions were manually segmented for size measurement and metrics for objective assessment of melanin distributions were calculated, including degree of polarization uniformity (DOPU), attenuation coefficient, and melanin occupancy rate (MOR).

Results. We imaged 17 patients (mean age = 69.5 years, range = 37–90) with 11 pigmented, 3 non-pigmented, and 3 mixed pigmentation nevi. Nevi with full margin acquisition had an average longest basal diameter of 5.1 mm (range = 2.99–8.72 mm) and average height of 0.72 mm (range = 0.37 mm–2.09 mm). PD-OCT provided clear contrast of choroidal melanin content, distribution, and delineation of nevus margins for melanotic nevi. Pigmented nevi were found to have lower DOPU, higher attenuation coefficient, and higher MOR than non-pigmented lesions. Melanin content on PD-OCT was consistent with pigmentation on fundus in 15 of 17 nevi (88%).

Conclusions. PD-OCT allows objective assessment of choroidal nevi melanin content and distribution. In addition, melanin-specific contrast by PD-OCT enables clear nevus margin delineation and may improve serial growth surveillance. Further investigation is needed to determine the clinical significance and prognostic value of melanin characterization by PD-OCT in the evaluation of choroidal nevi.

Keywords: optical coherence tomography (OCT), choroidal nevi, choroidal melanoma, polarization

Choroidal nevi are common benign intraocular neoplasms with a prevalence ranging from 0.15% to 6.5% depending on ethnicity.[1–5] Malignant transformation of a choroidal nevus to malignant choroidal melanoma has an estimated annual rate of 1 in 8845.[6] Prognosis for choroidal melanoma is poor, as approximately 50% of patients develop metastatic disease, and the 5-year mortality rate is 30%, although this varies depending on clinical staging.[7,8] Choroidal melanoma can spread micrometastases at an early stage; thus, long-term prognosis is improved with early diagnosis and treatment.[9,10] Clinical differentiation between benign choroidal nevi and choroidal melanoma requires thorough examination through multimodal imaging, which includes fundus photography, fluorescein angiography, indocyanine green angiography, fundus autofluorescence (FAF), optical coherence tomography (OCT), and ultrasonography (US).[11]

Whereas OCT has been extensively used for assessing choroidal nevi and the secondary changes affecting the overlying retina and choriocapillaris, it lacks tissue-specific contrast within the various layers of the eyes.[12,13] Polarization-sensitive OCT (PS-OCT) has been developed as

a functional extension of OCT that measures the polarization state of light.[13–17] The degree of polarization uniformity (DOPU) is a metric that has been developed to measure this depolarization and was found to increase as melanin concentration decreased.[13,14,18] Polarization-diversity OCT (PD-OCT) is a type of PS-OCT described in a previous study[19] that is capable of obtaining DOPU contrast in addition to scattering information attainable by conventional swept-source OCT imaging, which we refer to as "non-PD-OCT" in this paper. Based on the fact that melanin depolarizes light, PD-OCT provides tissue-specific contrast of retinal and choroid layers containing melanin.

Melanin is a pigment molecule produced by uveal melanocytes in the iris, ciliary body, and choroid, and by retinal pigment epithelial (RPE) cells, of which the RPE is the most studied.[20] Uveal melanin is believed to play a photoprotective role protecting melanocytes from oxidative stress, and is responsible for nevus pigmentation.[20] Up to 89% of choroidal nevi are pigmented,[21,22] whereas 5% to 10% are non-pigmented.[23,24] The terms "pigmented" and "melanotic" are often used interchangeably, however, we use "pigmented" to refer to fundus photograph appearance and "melanotic" to refer to melanin content on PD-OCT. Variation in nevi pigmentation can be attributed to their cellular composition, as there exist different subtypes of atypical melanocytes associated with different amounts of melanin.[25] Likewise, primary uveal melanomas are derived from the same cell population and thus also have varying pigmentation.[26,27] Clinical assessment of lesion pigmentation is typically done subjectively based on indirect ophthalmoscopy or fundus photography, which only provides a frontal projection of the retina with no depth-specific information.

In this study, we assess the utility of PD-OCT imaging of nevi in (1) objective assessment of lesion pigmentation and (2) margin delineation. For objective assessment of pigmentation, we perform quantitative analysis of nevus melanin signal on PD-OCT and determine its correlation to pigmentation on fundus photography. For margin delineation, we compare nevus margins delineated with DOPU signal on PD-OCT with margins delineated by scattering intensity on non-PD-OCT, as well as margins measured with US, which is the gold standard for clinical assessment of nevi. We hypothesize that intrinsic melanin content of nevi will be consistent with their pigmentation on fundus photograph, and melanin-specific contrast imaging through PD-OCT will distinguish nevus-specific, depth resolved lesion margins consistent with margins delineated with non-PD-OCT and ultrasonography.

Methods

Patient Recruitment and Data Collection

We performed a cross-sectional study of patients with choroidal nevi between October 2021 and August 2022 at 2 high-volume ophthalmology clinics in the Vancouver General Hospital (Vancouver, British Columbia, Canada). Patients diagnosed with at least one choroidal nevus were included in the study. Patients were given dilating eye drops (using 2.5% phenylephrine hydrochloride and 1% tropicamide) and underwent imaging with fundus photography (Topcon TRC-50DX, Topcon Corporation, Tokyo, Japan), auto-fluorescence (Optos P200dTx; Optos Inc., Marlborough, MA, USA, or Heidelberg Spectralis, Heidelberg Engineering Gmbh, Germany), and a research-prototype PD-OCT. Patients underwent formal ultrasonography (Aviso S; Quantel Medical, Bozeman, MT, USA) in all non-flat lesions as judged by clinical examination and commercial OCT imaging. Fundus pigmentation, presence of orange pigment on fundus autofluorescence, and PD-OCT features were evaluated independently by three ophthalmologists (authors K.S., K.P., and Z.M.). All patients were informed of the purpose and implications of the study, and written informed consent was obtained from each participant before participating in the study. This study was approved by the research ethics board at the University of British Columbia (human ethics protocol H19-03110) and followed the tenets of the Declaration of Helsinki.

System and Imaging Protocol

The PD-OCT system used in this study is based on our previous human retinal imaging swept-source OCT system[28] and illustrated in Supplementary Figure S1. The light source used is a vertical cavity surface emitting laser (VCSEL; SVM10F-0210; Thorlabs, Inc., Newton, NJ, USA), with an A-scan rate of 400 kHz, center wavelength of 1060 nm, and a bandwidth of 100 nm (-10 dB), providing an axial resolution of 7.06 µm in air. A custom-built retinal scanner was attached to the scanning arm, designed based on the 55-degree handheld OCT scanning head previously published.[29] The beam diameter at the pupil is measured to be 1.3 mm with sample power of 1.5 mW at the cornea. The OCT interference signal is digitized by a 12-bit waveform digitizer (ATS9373; AlazarTech Inc., Pointe-Claire, Quebec, Canada) with 1536 sampling points, allowing dual-channel acquisition at a rate of 1.5 Giga-samples/second. A bi-directional scanning pattern was used to perform high-speed raster scanning with a high duty cycle, with volume sizes of 1000 A-scans by 1000 B-scans, corresponding volume acquisition time of 2.5 seconds/volume.[30] Polarization diversity detection unit implemented in PD-OCT enables the measurement of an orthogonally polarized beam state (called the horizontal H- and vertical V-channels) of the detected signal via polarization beam splitter. This in turn is used to compute DOPU, which is a measure of the circular variance of Stokes vectors in a local region.[31,32] DOPU contrast determines the amount to which the polarization state of the input beam is preserved after interaction with the sample, with 1 indicating no change in polarization, and 0 being a completely randomized polarization state. In addition, a composite of two polarization channels in PD-OCT can be generated to produce a scattering intensity image, equivalent to a conventional OCT obtained by a commercial swept-source system, which we refer to as "non-PD-OCT."

Post-Processing and Multiparametric Characterization of Nevi

To differentiate tissue characteristics in choroidal nevi, we used a post-processing pipeline outlined in Supplementary Figure S2 to produce several nevi characterization metrics. The pre-processing step computes the complex OCT volumes of two polarization channels from the interference signals recorded from the two balanced detectors in PD-OCT, which is accompanied by wavenumber linearization,[33] numerical dispersion correction, and fast Fourier transformation. Non-PD OCT images were generated by taking composite of the complex OCT images acquired from two polariza-

tion channels after correcting the phase offset between the two channels. The complex OCT images from two polarization channels were converted to DOPU B-scans with the adaptive DOPU averaging kernel algorithm described in our previous study.[19] In this study, the size of the adaptive DOPU averaging kernel was set to 3 (axial) × 5 (lateral) pixels, empirically determined to provide optimal image quality. The resulting DOPU values undergo a final threshold and filtering with a three-dimensional median filter (3 × 3 × 3 pixels) to eliminate excess background noise. The DOPU en face maps were then generated by taking a minimum projection of DOPU values along the depth axis. The size of melanotic nevi was determined from the DOPU en face by manually segmenting regions of relatively lower DOPU compared to their surroundings. The area of the segmented regions was quantified in terms of the number of pixels, and the longest axis length was measured and converted to its physical length based on the resolution of the pixels.

Two additional metrics were introduced to quantitatively assess tissue properties in choroidal nevi. Attenuation coefficient was derived from non-PD-OCT images using the depth-resolved method proposed by Vermeer et al.,[34] which assesses the scattering and absorption properties of the targeted tissue. Melanin occupancy rate was derived from PD-OCT data and calculated as the percentage area of low-DOPU (<0.95) within the nevus margin. We created melanin distribution maps from DOPU B-scans by highlighting only the low-melanin area of each lesion. Note the calculation of melanin occupancy rate is similar to the method proposed by Miura et al.,[35] but the threshold value was modified as all of our patients are of Caucasian background, which is associated with lower choroidal melanin than people of Asian background.[36,37] Finally, the lesion corresponding to choroidal nevi was manually segmented from non-PD-OCT B-scans via a segmentation assistant software (ITK-Snap).[38] The segmentation mask was then applied to DOPU B-scans, attenuation B-scans, and melanin distribution map to get quantification metrics.

Results

We examined 17 nevi from 17 patients, of which 11 were pigmented, 3 were non-pigmented, and 3 had mixed pigmentation based on appearance on fundus photography. Patient demographics and all nevi clinical characteristics, including quantitative analysis of melanin features on PD-OCT are summarized in the Table.

Nevus pigmentation on fundus photography was consistent with melanin appearance on PD-OCT in 15 of 17 cases (88%). Figure 1 shows a pigmented nevus demonstrating a melanotic appearance on PD-OCT. Nevi with mixed pigmentation had a heterogenous melanin distribution on PD-OCT consistent with its fundus appearance, as shown in Figure 2, whereas these contrasting areas could not be

Table. Patient Demographics and Nevi Characteristics

Feature	Pigmented	Mixed	Non-Pigmented
Total number of nevi	11 (100)	3 (100)	3 (100)
Average age (SD)	68 (17)	84 (6)	61 (15)
Gender			
Male	5 (45)	1 (33)	2 (66)
Female	6 (55)	2 (66)	1 (33)
Involved eye			
Left	6 (55)	3 (100)	1 (33)
Right	5 (45)	0 (0)	2 (66)
Ethnicity Caucasian	11 (100)	3 (100)	3 (100)
Quadrantic location			
Macula	2 (18)	0 (0)	0 (0)
Inferior	1 (9)	1 (33)	1 (33)
Temporal	6 (55)	1 (33)	2 (66)
Superior	1 (9)	1 (33)	0 (0)
Nasal	1 (9)	0 (0)	0 (0)
Size measured with non-PD-OCT*			
Basal diameter, mm (SD)	4.56 (1.36)	5.65 (0.42)	6.33 (2.06)
Height, mm (SD)	0.58 (0.11)	0.57 (0.07)	1.23 (0.78)
Area, mm^2 (SD)	12.49 (6.81)	16.86 (3.79)	25.37 (16.43)
Subretinal fluid	4 (33)	0 (0)	1 (33)
Orange pigment on AF			
Yes	0 (0)	0 (0)	1 (33)
No	9 (82)	3 (100)	2 (67)
AF not available	2 (18)	0 (0)	0 (0)
RPE melanin loss on PD-OCT			
Yes	6 (55)	1 (33)	2 (50)
No	5 (45)	2 (66)	1 (50)
Mean DOPU (SD)	0.896 (0.080)	0.985 (0.017)	0.994 (0.010)
Mean attenuation coefficient (SD)	1.521 (0.650)	1.354 (0.421)	1.117 (0.284)
Melanin occupancy, % (SD)	47.2 (32.9)	15.6 (18.7)	6.42 (11.1)

Pigmentation was determined based on fundus photo appearance. Percentages are written in parentheses, unless otherwise specified.
SD, Standard deviation; AF, autofluorescence; PD-OCT, Polarization-diversity optical coherence tomography; DOPU, degree of polarization uniformity.
* Size measurement was not possible for two pigmented nevi and one mixed nevus due to incomplete margin acquisition.

Investigative Ophthalmology & Visual Science

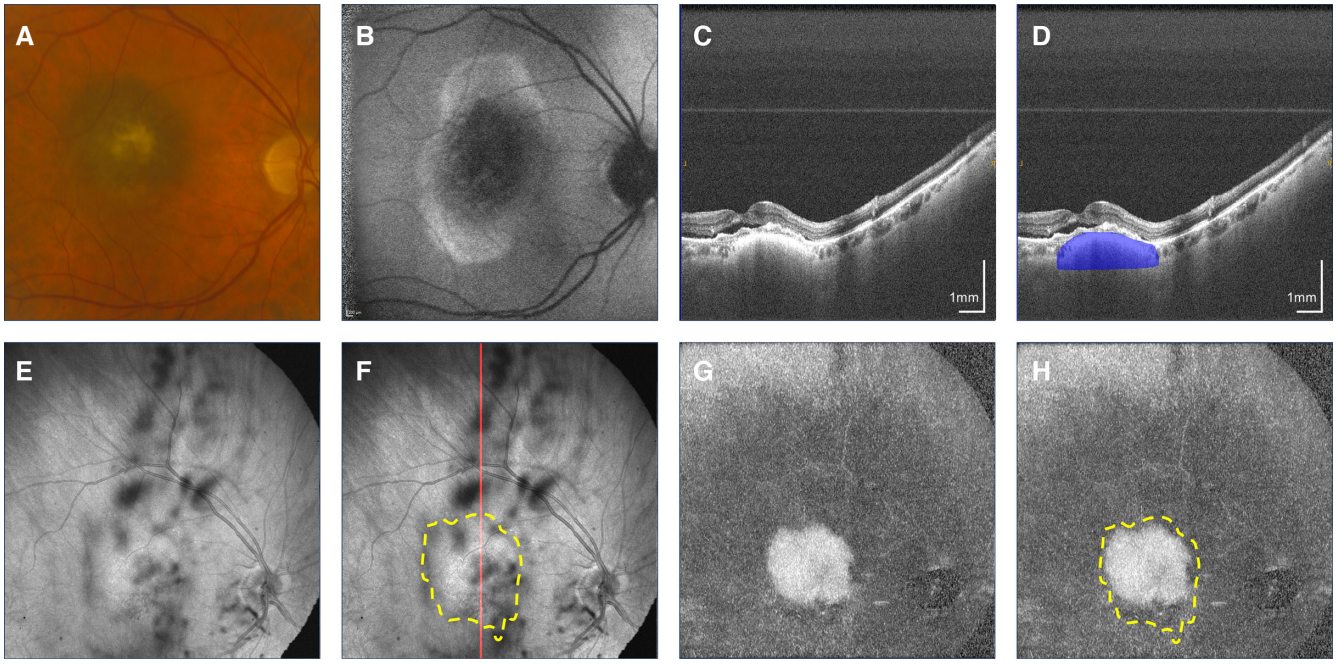

Figure 1. Macular pigmented choroidal nevus. (**A**) Fundus photograph. (**B**) Fundus autofluorescence. (**C, D**) Non-polarization-diversity optical coherence tomography (non-PD-OCT) en face B-scan, with an example margin segmentation shown in **D**. (**E, F**) Non-PD-OCT en face projection with margins segmented on non-PD-OCT B-scans shown as a *yellow overlay* in **F**. The *red line* indicates location of the B-scan shown in **C** and **D**. (**G, H**) Degree of polarization uniformity (DOPU) en face projection with margins segmented on non-PD-OCT B-scans shown as a *yellow overlay* in **H**.

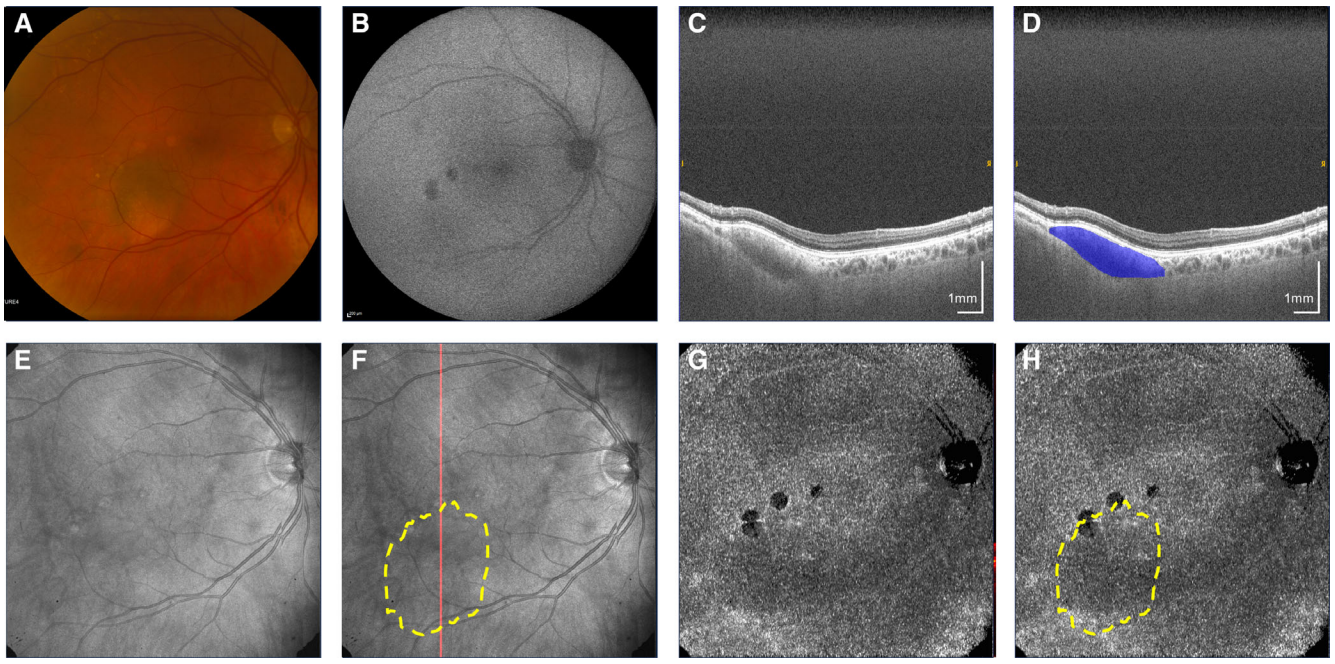

Figure 2. Mixed pigmentation nevus temporal to the macula. (**A**) Fundus photograph showing focal areas of chorioretinal atrophy superior to the lesion. (**B**) Fundus autofluorescence showing hypoautofluorescent signal along the areas of chorioretinal atrophy. (**C, D**) Non-polarization-diversity optical coherence tomography (non-PD-OCT) en face B-scan, with an example margin segmentation shown in **D**. (**E, F**) Non-PD-OCT en face projection, with margins segmented on non-PD-OCT B-scans shown as a *yellow overlay* in **F**. The *red line* indicates the location of the B-scan shown in **C** and **D**. (**G, H**) Degree of polarization uniformity (DOPU) en face projection, with margins segmented on non-PD-OCT B-scans shown as a *yellow overlay* in **H**.

distinguished on non-PD-OCT en face projection (see Fig. 2C). Non-pigmented nevi such as the case in Figure 3 demonstrated low melanin signal on PD-OCT and low light attenuation on non-PD-OCT and DOPU B-scan projections (see Figs. 3E, 3G), with adequate light penetration for visualization of the scleral boundary. Pigmented lesions were asso-

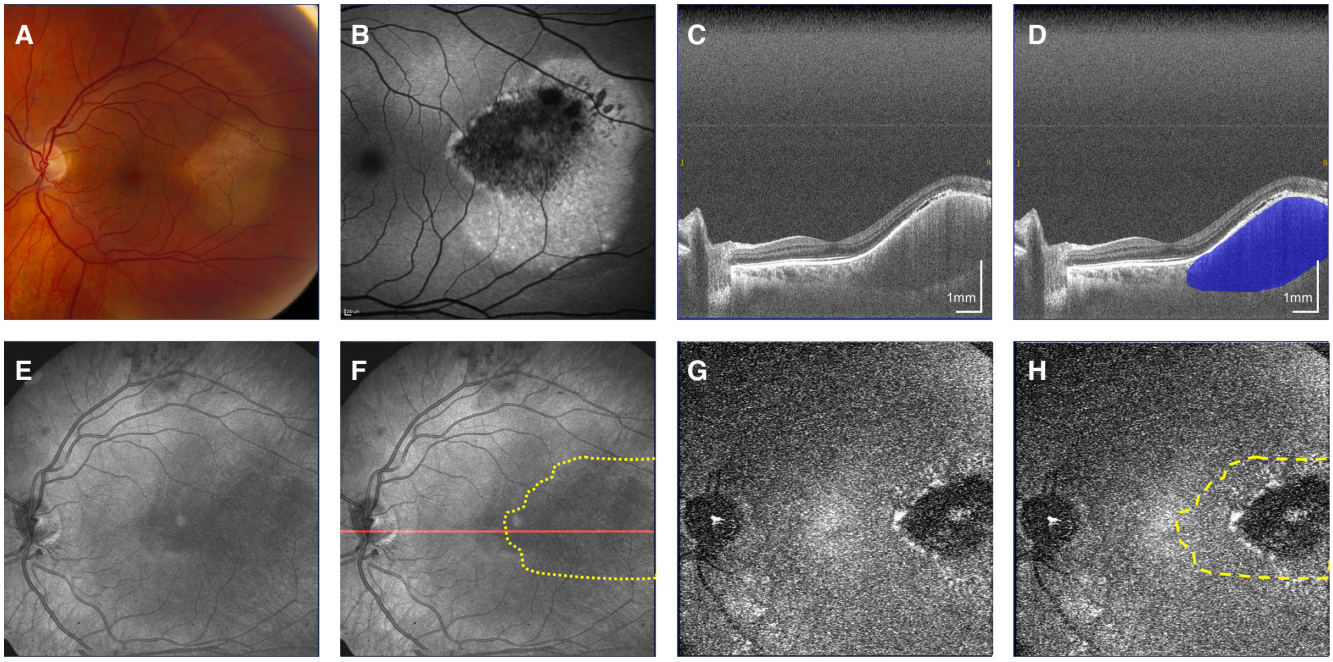

Figure 3. Non-pigmented nevus temporal to the macula. (**A**) Fundus photograph. (**B**) Fundus autofluorescence. (**C, D**) Non-polarization-diversity optical coherence tomography (non-PD-OCT) en face B-scan, with an example margin segmentation shown in **D**. (**E, F**) Non-PD-OCT en face projection, with margins segmented on non-PD-OCT B-scans shown as a *yellow overlay* in **F**. The *red line* indicates location of the B-scan shown in **C** and **D**. (**G, H**) Degree of polarization uniformity (DOPU) en face projection, with margins segmented on non-PD-OCT B-scans shown as a *yellow overlay* in **H**.

ciated with lower DOPU, higher melanin occupancy, and higher attenuation coefficients than non-pigmented lesions (Fig. 4). We identified two cases with a discrepancy between fundus pigmentation and melanin appearance on PD-OCT. Both cases appeared pigmented on fundus photograph but primarily amelanotic with some melanotic regions on PD-OCT, an example is shown in Figure 5. These nevi demonstrated low attenuation, high DOPU, and low melanin occupancy, similar to other amelanotic nevi in our study. Otherwise, 9 of 11 (82%) of pigmented lesions had a corresponding melanotic appearance on PD-OCT, 3 of 3 (100%) mixed pigmentation cases had mixed melanin appearance on PD-OCT, and 3 of 3 (100%) non-pigmented cases had amelanotic appearance on PD-OCT.

Height, basal diameter, and area measurements of nevi were obtained by manual segmentation of non-PD-OCT B-scans. As two pigmented nevi and one mixed nevus did not have full margin acquisition, size measurement was not performed for these cases. The remaining 14 nevi imaged with full margin acquisition had an average longest basal diameter of 5.1 mm (range = 2.99–8.72 mm), average height of 0.72 mm (range = 0.37 mm–2.09 mm), and area of 15.87 mm^2 (range = 3.92–42.78 mm^2). Figure 2 shows a pigmented nevus with a well-circumscribed margin on DOPU en face projection (see Fig. 2D) consistent with its appearance on fundus photograph (see Fig. 2A), whereas margins are not as clear on non-PD-OCT en face projection (see Fig. 2C). Nonpigmented nevi had poor margin delineation on PD-OCT, except for a case shown in Figure 4, in which concurrent melanin loss in the RPE caused the nevus to have a lower melanin signal on PD-OCT en face projection compared to the surrounding choroid. Similar to the pigmented nevi, this enabled margin delineation on PD-OCT, whereas these contrasting areas could not be distinguished on non-PD-OCT en face projection. To further evaluate the accuracy of margin assessment with PD-OCT, we compared the measurements of lesion area and height obtained from non-PD-OCT, DOPU, and US images. Figure 6A shows the comparison of lesion area measurements from volume segmentation of non-PD-OCT versus DOPU en face projection image in 11 pigmented nevi. Nevus margin delineation with segmentation of single DOPU en face projections yielded similar size measurements, despite requiring significantly less manual labor, than margin delineation with whole-volume segmentation of non-PD-OCT B-scans. Segmentation of non-PD-OCT en face projections were not possible due to poor margin visualization in the majority of cases in our cohort. Of 11 pigmented nevi, 8 had a smaller area measurement on PD-OCT compared to non-PD-OCT, with an average difference of −0.8 mm^2 (range = −8.0 mm^2 to 5.7 mm^2. Furthermore, lesion height measurements on US were compared to that on non-PD-OCT in 11 non-flat nevi. Nevi height measured on non-PD-OCT B-scan were found to be generally lower than the height measured on US especially in smaller nevi, although larger nevi were found to have better concordance of apical height measurements between US and non-PD-OCT (see Fig. 6B). Of these 11 non-flat nevi, 10 cases had a greater height measurement on ultrasound compared to non-PD-OCT, with average difference of 0.5 mm (range = −0.19 mm to −0.80 mm) between the 2 methods. Bland-Altman plots showing the agreeability in area and height measurements between different modalities are shown in Supplementary Figures S3 and S4, respectively. The lesion height comparison between US and PD-OCT was not conducted in this study due to the small number of pigmented nevi cases ($N = 6$) that also had US taken.

Investigative Ophthalmology & Visual Science

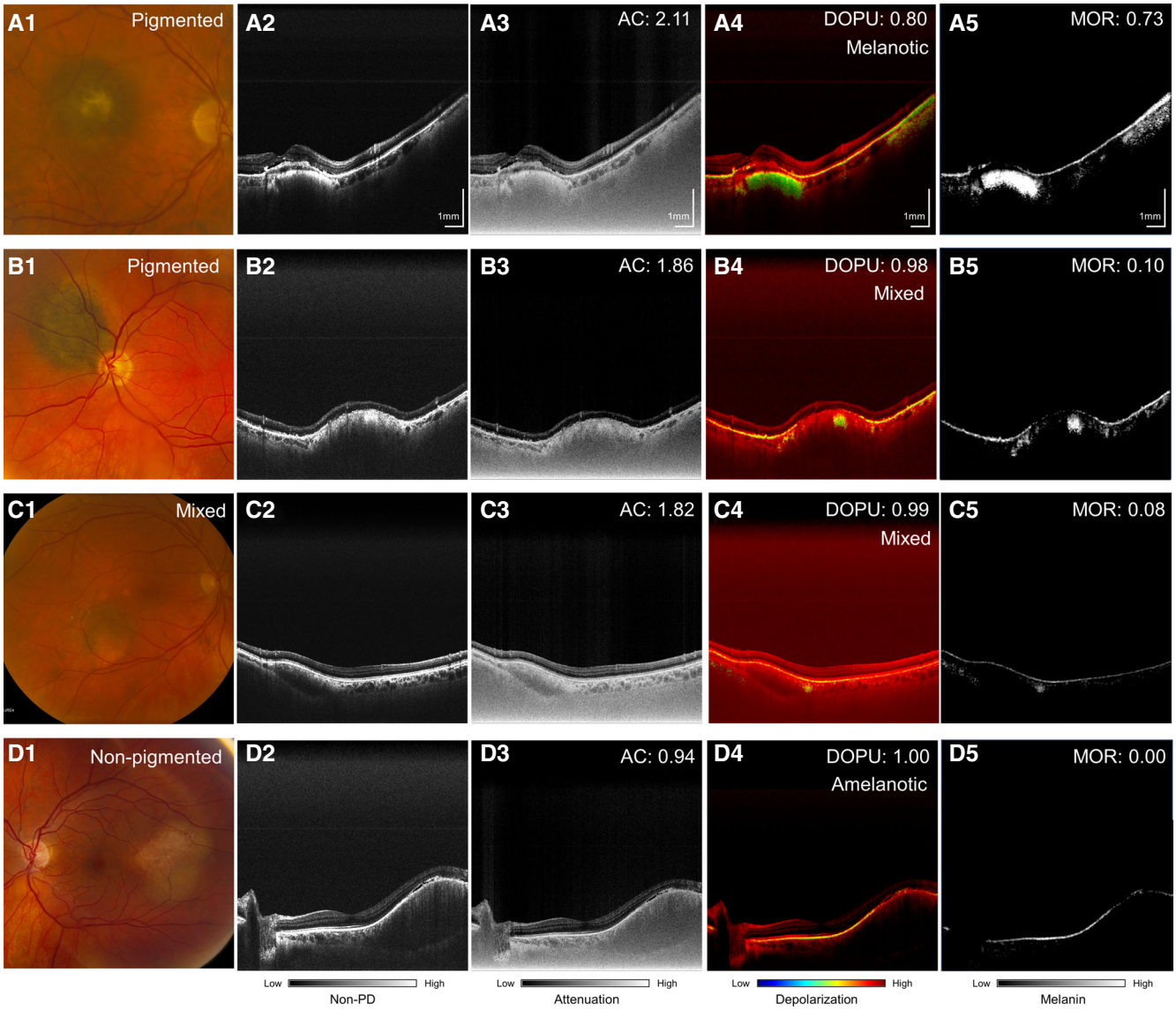

Figure 4. Quantitative assessment of nevi from polarization-diversity optical coherence tomography (PD-OCT). *Column 1*: Fundus photograph. *Column 2*: Non-PD-OCT B-scan with linear scale representation. *Column 3*: Attenuation coefficient (AC) projection. *Column 4*: Degree of polarization uniformity (DOPU) projection. *Column 5*: Melanin occupancy rate (MOR) projection. Shown are example cases of a pigmented nevus (row **A**), pigmented nevus with mixed melanotic/amelanotic appearance on PD-OCT (row **B**), mixed pigmentation nevus (row **C**), and non-pigmented nevus (row **D**) are shown.

Discussion

In this study, we have demonstrated PD-OCT-enabled objective assessment of choroidal nevus melanin content and clear margin characterization. Melanin contrast imaging through PD-OCT provides visualization of superficial and deep melanin within the RPE and choroid. In addition to melanin contrast, the scattering contrast used by PD-OCT enables visualization of the hyperreflective RPE, the anterior nevus margin, as well as secondary retinal changes such as subretinal fluid, shaggy photoreceptors, and drusen.[39]

Nevus pigmentation is typically assessed subjectively through fundus photography, which can also provide information regarding nevi size and location, but only provides a frontal projection and no depth-specific pigmentation information. Although non-PD-OCT is not used to determine pigmentation, pigmented nevi generally demonstrate increased reflectivity and optical shadowing compared to non-pigmented nevi,[40] which is consistent with our findings. Although 88% of our cases demonstrated melanin content on PD-OCT consistent with fundus pigmentation, we identified two cases in which nevi appeared pigmented on fundus photograph but appeared primarily amelanotic with some melanotic regions on PD-OCT. Given their low melanin signal, it is possible that the presence of other dense tissue material within these nevi are responsible for their pigmentation and increased light attenuation, such as necrotic tissue.[41] Therefore, although nevus pigmentation on fundus photograph is consistent with its melanin content in the majority of cases, they are not necessarily interchangeable. Given our limited sample size with three mixed pigmentation nevi and three non-pigmented nevi,

Investigative Ophthalmology & Visual Science

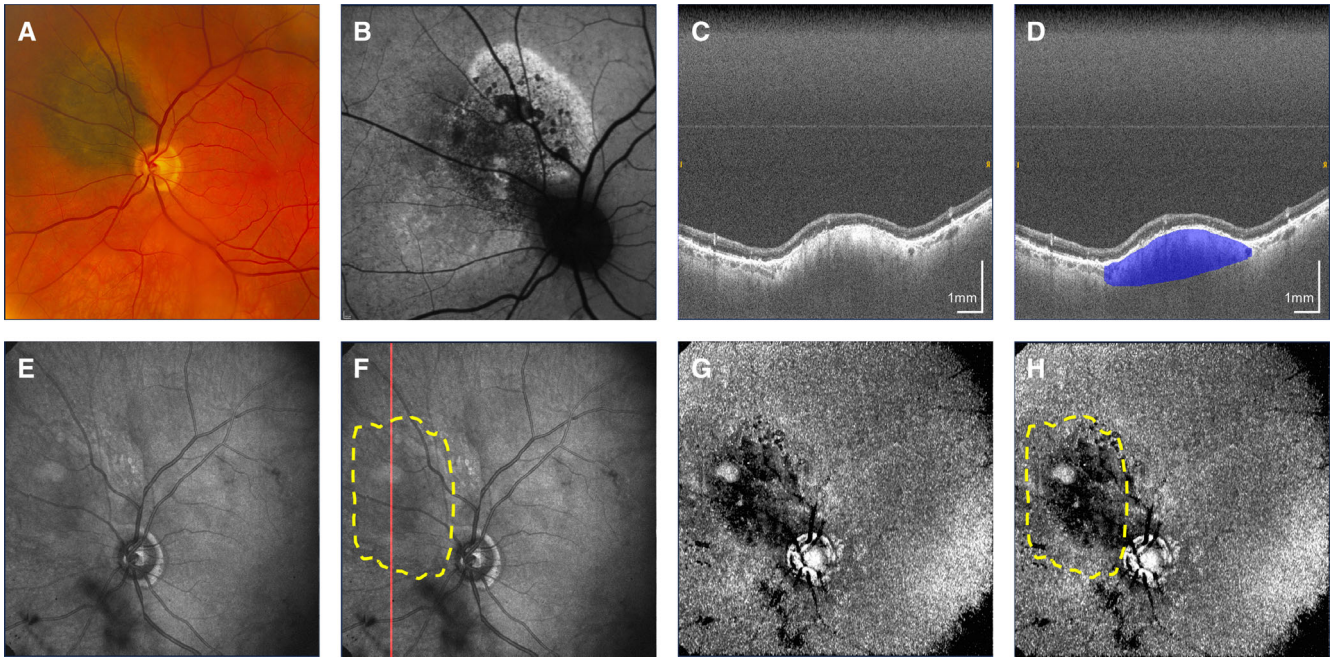

Figure 5. Juxtapapillary pigmented nevus. (**A**) Fundus photograph. (**B**) Fundus autofluorescence. (**C, D**) Non-polarization-diversity optical coherence tomography (non-PD-OCT) en face B-scan, with an example margin segmentation shown in **D**. (**E, F**) Non-PD-OCT en face projection, with margins segmented on non-PD-OCT B-scans shown as a *yellow overlay* in **F**. The *red line* indicates B-scan shown in **C** and **D**. (**G, H**) Degree of polarization uniformity (DOPU) en face projection showing a mixed melanotic/amelanotic appearance despite pigmented appearance on fundus, with margins segmented on non-PD-OCT B-scans shown as a *yellow overlay* in **H**.

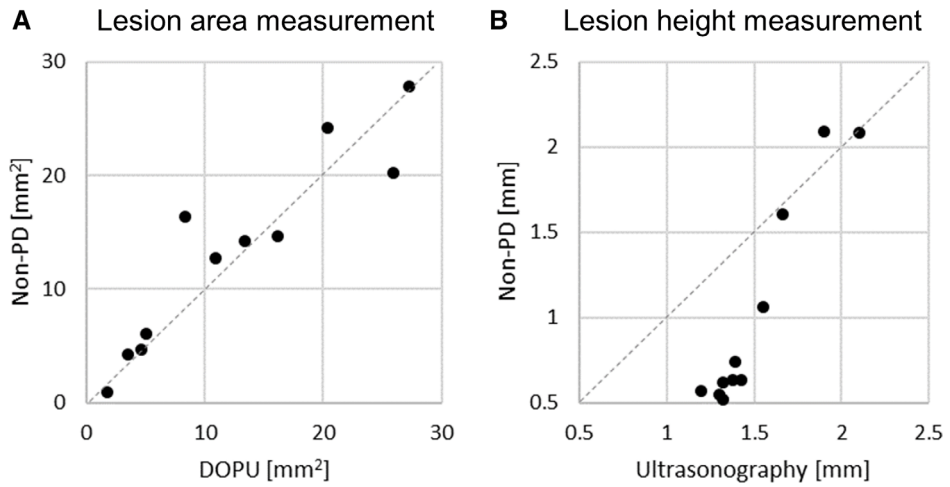

Figure 6. Comparison of margins assessed with non-polarization-diversity optical coherence tomography (non-PD-OCT) B-scans, degree of polarization uniformity (DOPU) en face projections, or ultrasonography. (**A**) Nevi area measurement based on DOPU en face and non-PD-OCT volume segmentation of pigmented nevi ($N = 11$). (**B**) Nevi height measurement based on ultrasonography and non-PD-OCT volume segmentation ($N = 11$). Of 17 nevi in our cohort, 11 underwent ultrasonographic imaging (6 pigmented, 3 mixed pigmentation, and 2 non-pigmented).

further imaging of nevi with varying pigmentation can help to elucidate the true relationship between fundus pigmentation and intrinsic melanin content. Future studies may also investigate whether there is a discrepancy between fundus pigmentation and melanin appearance on PD-OCT of other pathologies, such as melanoma or choroidal metastases.

Nevus height and basal diameter are important clinical considerations in stratifying risk of malignant transformation and monitoring for growth.[42] We demonstrated that lesion size measured based on scattering contrast with non-PD-OCT was consistent with lesion size measured based on melanin contrast with PD-OCT. Furthermore, height of lesions measured through manual segmentation of non-PD-OCT images was consistent with the height measured by US for lesions of height greater than 1.5 mm, however, smaller nevi measured with US had a greater apparent height than when measured with non-PD-OCT. The discrepancy in the height measurements between OCT and US in the case of

smaller size nevi is likely attributed to the differences in axial resolution, as the axial resolution of OCT ranges from 1 to 15 µm whereas the axial resolution of typical ophthalmic US is around 450 µm.[43,44] This is consistent with findings reported in previous studies,[45,46] thus the height of smaller lesions is best measured with OCT, especially those under 1 mm.[47] Given the limited depth resolution of OCT, increased light attenuation by large, melanotic lesions can impede visualization of the scleral boundary.[39] For such larger cases, US is generally preferred over OCT for determining lesion height.

Our cohort was entirely comprised of patients of Caucasian ethnicity, whose low background choroidal melanin[37] provided a high degree of contrast with the strong melanin signal of melanotic nevi imaged with PD-OCT. This enabled margin visualization on PD-OCT based on difference in the melanin content between the lesion and the surrounding healthy choroid and RPE, whereas this contrast was not visible on non-PD-OCT images. As amelanotic nevi have a lower melanin content, margins were generally poorly defined with PD-OCT in two of three cases. An exception is the amelanotic nevus in Figure 5, in which there was concurrent loss of melanin in the RPE overlying the lesion, which caused the melanin signal of the lesion on PD-OCT en face projection to appear lower than the surrounding part. However, it is important to note that the region of melanin loss in the RPE does not necessarily correspond to the extent of the nevus itself. Further adding to this, nevi can be comprised of a heterogenous population of melanotic and amelanotic cells,[48] thus the melanotic region of a nevus visualized by PD-OCT may not necessarily represent the entire lesion area. Nevertheless, melanin contrast imaging provides an additional dimension to the clinical assessment of choroidal nevi, and when combined other acknowledged clinical characteristics of nevi including thickness, diameter, and subretinal fluid, may be a useful tool for the longitudinal assessment of nevi for growth. Serial follow-up imaging of nevi with PD-OCT is needed to determine whether melanin distribution patterns change over time and if these changes are associated with lesion growth. The development of advanced segmentation techniques to isolate layer-specific melanin signal may also improve assessment of melanin changes in these regions over time.

We demonstrated that the size and shape of melanotic nevi with diameter between 3 and 8 mm can be reliably assessed using our PD-OCT system. Furthermore, a 55-degree wide scanning angle retinal scanner combined with high-speed swept-source laser was implemented to achieve an unprecedented wide FOV. Supplementary Table S1 summarizes the imaging protocols of similar PS-OCT and PD-OCT systems in terms of FOV, A-line speed, and acquisition time. Having a large FOV not only helps to capture relatively large choroidal lesions but also minimizes the requirement of operator input to identify nevi located in the peripheral retina.

We have demonstrated that depth-resolved ocular melanin visualized by PD-OCT can be further assessed through objective measures including DOPU, attenuation coefficient, and MOR. Pigmented nevi demonstrated lower DOPU values, higher light attenuation, and higher melanin occupancy than nonpigmented nevi. In particular, MOR was found to differ widely among pigmented lesions, likely due to the highly scattering nature of pigmented lesions preventing adequate light penetration to visualize melanin down to the scleral boundary of elevated lesions. Although we demonstrate that PD-OCT can enable objective assessment of ocular melanin, further studies are needed to refine our understanding of how melanin synthesis and distribution are implicated in the pathogenesis of choroidal nevi and melanomas.

Although PD-OCT confers unique advantages in enabling melanin-specific contrast imaging of the posterior retina and choroid, this imaging modality comes with several limitations. First, although our system is the largest FOV PD-OCT system published to date, the FOV is still limited compared to that of a commercial wide field scanning laser ophthalmoscope which can have an FOV of up to 200 degrees. As a result, full margin acquisition of choroidal lesions located near the equator with our PD-OCT system remains a challenge. A previous study has suggested that an FOV of more than 100 degrees is desirable for a reduction in total imaging time and detecting peripheral retinal pathologies.[49] Furthermore, limitations in measurable depth range at a given illumination power made it challenging to visualize the scleral boundary and measure the height of highly scattering melanotic nevi. Given our small sample size and low number of mixed pigmentation and non-pigmented nevi, an increased sample size may further elucidate differences in PD-OCT imaging features of different pigmentation groups of nevi. As mentioned previously, all patients in our study are Caucasian, therefore, we cannot validate whether our objective assessment of melanin and nevus margin delineation is affected by race-based differences in choroidal melanin.[36,37] DOPU is also dependent on the polarization state of the incident light, which may prevent extrapolation of DOPU values across different patients. Previous studies have introduced the computation of entropy as well as depolarization index, which are insensitive to incident polarization state, as a reproducible parameter to report melanin quantity.[17,50–52]

Conclusions

In this study, we demonstrated that melanin-specific contrast provided by PD-OCT can be useful in assessing lesion margin, melanin content, and size, in addition to visualization of secondary retinal changes with scattering contrast. En face intensity projection of DOPU showed clear delineation of melanotic nevi margins, as well as some amelanotic nevi in patients with high baseline choroidal melanin. In future studies, advanced image segmentation techniques can be integrated to improve lesion margin visualization of amelanotic nevi. Compared to conventional imaging modalities, PD-OCT enables objective assessment of melanin in choroidal lesions. Further imaging with a larger sample size can correlate nevus pigmentation on fundus photograph with objective melanin parameters measured by PD-OCT, including attenuation coefficient, DOPU, and MOR. Serial follow-up imaging is needed to determine whether melanin distribution patterns of nevi are associated with lesion growth. Further studies are also needed to refine our understanding of how melanin distribution within nevi is implicated in tumor pathogenesis and risk of malignant transformation.

Acknowledgments

Supported in part by Michael Smith Health Research BC (Canada); The Paul and Edwina Heller Memorial Fund (Canada), in part by Natural Sciences and Engineering Research Council of Canada (Canada), in part by Canadian Institutes of Health Research (Canada), in part by the Alzheimer Society Research

Program (Canada), in part by Canada Foundation for Innovation (Canada), in part by Canadian Cancer Society (Canada), and in part by Brain Canada Foundation (Canada).

Disclosure: **Y. Miao,** None; **H. Jung,** None; **D. Hsu,** None; **J. Song,** None; **S. Ni,** None; **D. Ma,** None; **Y. Jian,** Seymour Vision Inc. (I); **S. Makita,** Nikon (F), Sky Technology (F), Yokogawa Electric Corp. (F), Kao Corp. (F), Topcon (F); **Y. Yasuno,** Nikon (F), Sky Technology (F), Yokogawa Electric Corp. (F), Kao Corp. (F), Topcon (F); **M.V. Sarunic,** Seymour Vision Inc. (I); **K.A.J. Stephenson**, None; **K. Paton,** None; **Z. Mammo,** None; **M.J. Ju,** None

References

1. Qiu M, Shields CL. Choroidal nevus in the United States adult population. *Ophthalmology*. 2015;122(10):2071–2083.
2. Jonas JB, You QS, Xu L, Wang YX. Choroidal nevi in adult Chinese. *Ophthalmology*. 2008;115(6):1102–1102.e1.
3. Ng CH, Wang JJ, Mitchell P, Amirul Islam FM, Wong TY. Prevalence and characteristics of choroidal nevi in an Asian vs White population. *Arch Ophthalmol*. 2009;127(3):314–319.
4. Nangia V, Jonas JB, Agarwal S, Khare A, Lambat S, Panda-Jonas S. Choroidal nevi in adult Indians: the Central India Eye and Medical Study. *Br J Ophthalmol*. 2012;96(11):1443–1444.
5. Sumich P, Mitchell P, Wang JJ. Choroidal nevi in a white population: the Blue Mountains Eye Study. *Arch Ophthalmol*. 1998;116(5):645–650.
6. Singh AD, Kalyani P, Topham A. Estimating the risk of malignant transformation of a choroidal nevus. *Ophthalmology*. 2005;112(10):1784–1789.
7. Straatsma B, Diener-West M, Caldwell R, Engstrom R, for the Collaborative Ocular Melanoma Study Group. Mortality after deferral of treatment or no treatment for choroidal melanoma. *Indian J Ophthalmol*. 2018;66(10):1395.
8. Kujala E, Mäkitie T, Kivela T. Very long-term prognosis of patients with malignant uveal melanoma. *Invest Ophthalmol Vis Sci*. 2003;44(11):4651.
9. Eskelin S, Pyrhönen S, Summanen P, Hahka-Kemppinen M, Kivelä T. Tumor doubling times in metastatic malignant melanoma of the uvea: tumor progression before and after treatment. *Ophthalmology*. 2000;107(8):1443–1449.
10. Shields CL. Metastasis of uveal melanoma millimeter-by-millimeter in 8033 consecutive eyes. *Arch Ophthalmol*. 2009;127(8):989.
11. Shields CL, Pellegrini M, Ferenczy SR, Shields JA. Enhanced depth imaging optical coherence tomography of intraocular tumors: from placid to seasick to rock and rolling topography—the 2013 Francesco Orzalesi lecture. *Retina*. 2014;34(8):1495–1512.
12. Shields CL, Materin MA, Shields JA. Review of optical coherence tomography for intraocular tumors: *Curr Opin Ophthalmol*. 2005;16(3):141–154.
13. Baumann B, Baumann SO, Konegger T, et al. Polarization sensitive optical coherence tomography of melanin provides intrinsic contrast based on depolarization. *Biomed Opt Express*. 2012;3(7):1670.
14. Pircher M, Hitzenberger CK, Schmidt-Erfurth U. Polarization sensitive optical coherence tomography in the human eye. *Prog Retinal Eye Res*. 2011;30(6):431–451.
15. Yamanari M, Matsuzaki M, Takagi S, et al. Polarization-sensitive swept-source OCT imaging of retinal pigment epithelium and subretinal fibrous tissues. *Invest Ophthalmol Vis Sci*. 2018;59(9):291.
16. Sakai D, Takagi S, Totani K, et al. Retinal pigment epithelium melanin imaging using polarization-sensitive optical coherence tomography for patients with retinitis pigmentosa. *Sci Rep*. 2022;12:7115.
17. Yamanari M, Mase M, Obata R, et al. Melanin concentration and depolarization metrics measurement by polarization-sensitive optical coherence tomography. *Sci Rep*. 2020;10(1):19513.
18. Götzinger E, Pircher M, Geitzenauer W, et al. Retinal pigment epithelium segmentation by polarization sensitive optical coherence tomography. *Opt Express*. 2008;16(21):16410.
19. Hsu D, Kwon JH, Ng R, et al. Quantitative multi-contrast in vivo mouse imaging with polarization diversity optical coherence tomography and angiography. *Biomed Opt Express*. 2020;11(12):6945–6961.
20. Hu DN, Simon JD, Sarna T. Role of ocular melanin in ophthalmic physiology and pathology†. *Photochem Photobiol*. 2008;84(3):639–644.
21. Shah SU, Kaliki S, Shields CL, Ferenczy SR, Harmon SA, Shields JA. Enhanced depth imaging optical coherence tomography of choroidal nevus in 104 cases. *Ophthalmology*. 2012;119(5):1066–1072.
22. Shields CL, Furuta M, Mashayekhi A, et al. Clinical spectrum of choroidal nevi based on age at presentation in 3422 consecutive eyes. *Ophthalmology*. 2008;115(3):546–552.e2.
23. Hage DG, Wahab CH, Kheir WJ. Choroidal sarcoid granuloma: a case report and review of the literature. *J Ophthal Inflamm Infect*. 2022;12(1):31.
24. Welch RJ, Newman JH, Honig SE, et al. Choroidal amelanotic tumours: clinical differentiation of benign from malignant lesions in 5586 cases. *Br J Ophthalmol*. 2020;104(2):194–201.
25. Naumann G, Yanoff M, Zimmerman LE. Histogenesis of malignant melanomas of the uvea. I. Histopathologic characteristics of nevi of the choroid and ciliary body. *Arch Ophthalmol*. 1966;76(6):784–796.
26. Histopathologic characteristics of uveal melanomas in eyes enucleated from the collaborative ocular melanoma study COMS report no. 6. *Am J Ophthalmol*. 1998;125(6):745–766.
27. Pandiani C, Béranger GE, Leclerc J, Ballotti R, Bertolotto C. Focus on cutaneous and uveal melanoma specificities. *Genes Dev*. 2017;31(8):724–743.
28. Ju MJ, Hsu D, Kwon JH, et al. Multi-scale and -contrast sensorless adaptive optics optical coherence tomography. *Quant Imaging Med Surg*. 2019;9(5):757–768.
29. Ni S, Wei X, Ng R, et al. High-speed and widefield handheld swept-source OCT angiography with a VCSEL light source. *Biomed Opt Express*. 2021;12(6):3553.
30. Ju MJ, Heisler M, Athwal A, Sarunic MV, Jian Y. Effective bidirectional scanning pattern for optical coherence tomography angiography. *Biomed Opt Express*. 2018;9(5):2336.
31. Makita S, Hong YJ, Miura M, Yasuno Y. Degree of polarization uniformity with high noise immunity using polarization-sensitive optical coherence tomography. *Opt Lett*. 2014;39(24):6783.
32. Makita S, Mino T, Yamaguchi T, Miura M, Azuma S, Yasuno Y. Clinical prototype of pigment and flow imaging optical coherence tomography for posterior eye investigation. *Biomed Opt Express*. 2018;9(9):1564–1571.
33. Yasuno Y, Madjarova VD, Makita S, et al. Three-dimensional and high-speed swept-source optical coherence tomography for in vivo investigation of human anterior eye segments. *Optics Express*. 2005;13(26):10652.
34. Vermeer KA, Mo J, Weda JJA, Lemij HG, de Boer JF. Depth-resolved model-based reconstruction of attenuation coefficients in optical coherence tomography. *Biomed Opt Express*. 2014;5(1):322.
35. Miura M, Makita S, Yasuno Y, et al. Evaluation of choroidal melanin-containing tissue in healthy Japanese subjects by

Investigative Ophthalmology & Visual Science

polarization-sensitive optical coherence tomography. *Sci Rep*. 2022;12(1):4048.
36. Houtzagers LE, Wierenga APA, Ruys AAM, Luyten GPM, Jager MJ. Iris colour and the risk of developing uveal melanoma. *Int J Mol Sci*. 2020;21(19):7172.
37. Harbour JW, Brantley MA, Hollingsworth H, Gordon M. Association between choroidal pigmentation and posterior uveal melanoma in a White population. *Br J Ophthalmol*. 2004;88(1):39–43.
38. Yushkevich PA, Piven J, Hazlett HC, et al. User-guided 3D active contour segmentation of anatomical structures: significantly improved efficiency and reliability. *Neuroimage*. 2006;31(3):1116–1128.
39. Solnik M, Paduszyńska N, Czarnecka AM, et al. Imaging of uveal melanoma—current standard and methods in development. *Cancers*. 2022;14(13):3147.
40. Vazquez-Alfageme C, Papastefanou VP, Patel PJ, Degli-Esposti S, Cohen VML, Sagoo MS. Swept-source OCT and near-infrared reflectance patterns in choroidal nevi. *Ophthalmol Retina*. 2019;3(5):429–435.
41. Gelmi MC, Wierenga APA, Kroes WGM, et al. Increased histological tumor pigmentation in uveal melanoma is related to eye color and loss of chromosome 3/BAP1. *Ophthalmol Sci*. 2023;3(3):100297.
42. Shields CL, Dalvin LA, Ancona-Lezama D, et al. Choroidal nevus imaging features in 3,806 cases and risk factors for transformation into melanoma in 2,355 cases: the 2020 Taylor R. Smith and Victor T. Curtin lecture. *Retina*. 2019;39(10):1840–1851.
43. Fujimoto JG, Pitris C, Boppart SA, Brezinski ME. Optical coherence tomography: an emerging technology for biomedical imaging and optical biopsy. *Neoplasia*. 2000;2(1–2):9–25.
44. Silverman RH. High-resolution ultrasound imaging of the eye – a review. *Clin Exp Ophthalmol*. 2009;37(1):54–67.
45. Collaborative Ocular Melanoma Study Group. Comparison of clinical, echographic, and histopathological measurements from eyes with medium-sized choroidal melanoma in the Collaborative Ocular Melanoma Study: COMS Report No. 21. *Arch Ophthalmol*. 2003;121(8):1163.
46. Jonna G, Daniels AB. Enhanced depth imaging OCT of ultrasonographically flat choroidal nevi demonstrates 5 distinct patterns. *Ophthalmol Retina*. 2019;3(3):270–277.
47. Kivelä T. Diagnosis of Uveal Melanoma. In: Jager MJ, Desjardins L, Kivelä T, Damato BE, eds. *Dev Ophthalmol*. Basel: S. Karger AG; 2012;49:1–15.
48. Lee DS, Anderson SF, Perez EM, Townsend JC. Amelanotic choroidal nevus and melanoma: cytology, tumor size, and pigmentation as prognostic indicators. *Optom Vis Sci*. 2001;78(7):483–491.
49. Ni S, Nguyen TTP, Ng R, et al. 105° field of view non-contact handheld swept-source optical coherence tomography. *Opt Lett*. 2021;46(23):5878.
50. Yamanari M, Tsuda S, Kokubun T, et al. Estimation of Jones matrix, birefringence and entropy using Cloude-Pottier decomposition in polarization-sensitive optical coherence tomography. *Biomed Opt Express*. 2016;7(9):3551.
51. Fujita A, Amari T, Ueda K, et al. Three-dimensional distribution of fundus depolarization and associating factors measured using polarization-sensitive optical coherence tomography. *Trans Vis Sci Tech*. 2021;10(2):30.
52. Lippok N, Braaf B, Villiger M, Oh WY, Vakoc BJ, Bouma BE. Quantitative depolarization measurements for fiber-based polarization-sensitive optical frequency domain imaging of the retinal pigment epithelium. *J Biophotonics*. 2019;12(1):e201800156.

Investigative Ophthalmology & Visual Science